Photoluminescence and ratiometric thermo-response of Eu^{2+} and Eu^{3+} in $BaAl_2B_2O_7:Eu^{2+},Eu^{3+}$ phosphor materials

Wang, Ziyao; Fu, Haitao; Zhan, Xiufeng; Tong, Bo; Ma, Guofeng; Hintzen, H. T.(Bert)

DOI
10.1016/j.jre.2023.06.017

Publication date
2024

Document Version
Final published version

Published in
Journal of Rare Earths

Journal of Rare Earths 42 (2024) 1240–1249

Contents lists available at ScienceDirect

Journal of Rare Earths

journal homepage: http://www.journals.elsevier.com/journal-of-rare-earths

Photoluminescence and ratiometric thermo-response of Eu^{2+} and Eu^{3+} in $BaAl_2B_2O_7$:Eu^{2+},Eu^{3+} phosphor materials☆

Ziyao Wang [a,*], Haitao Fu [b], Xiufeng Zhan [b], Bo Tong [b], Guofeng Ma [a], H.T. (Bert) Hintzen [c,**]

[a] Institute of Innovative Science and Technology, Shenyang University, Shenyang, 110044, China
[b] College of Mechanical Engineering, Shenyang University, Shenyang, 110044, China
[c] Faculty of Applied Sciences, Delft University of Technology, 2629 JB, Delft, the Netherlands

ARTICLE INFO

Article history:
Received 13 March 2023
Received in revised form
2 June 2023
Accepted 26 June 2023
Available online 19 August 2023

Keywords:
Photoluminescence
Ratiometric thermo-response
Phosphor
Eu^{2+}/Eu^{3+}
Rare earths

ABSTRACT

A novel Eu^{2+}-Eu^{3+} co-activated ratiometric thermo-sensitive phosphor was developed and synthesized by solid-state reaction. The valence state of Eu, photoluminescence and thermo-sensitive performance of the phosphor prepared either in ambient air or carbothermally were investigated and discussed. The phosphor shows high sensitivity (S_a = 0.0173 K^{-1}, S_r = 0.461%/K) and superior signal discriminability ($\Delta\nu$ ~10380 cm^{-1}). The thermo-sensitive performance is subject to the dual effects of different thermo-responses by Eu^{2+} versus Eu^{3+} combined with energy transfer from Eu^{2+} to Eu^{3+}, so that the sensitivity of the phosphor in the temperature range presents a non-monotonic trend. The development of the $BaAl_2B_2O_7$:Eu^{2+},Eu^{3+} phosphor is not only expected to be relevant for application in the field of temperature sensing, but also of reference significance for improving the sensitivity by means of energy transfer between co-activator ions over a wider temperature range of Eu^{2+}-Eu^{3+} co-activated ratiometric thermo-sensitive phosphors.

1. Introduction

As a general temperature signal converter, the temperature sensor has a large number of application scenarios in the fields of medical and health, food processing, metallurgy, printing and dyeing, and so on.[1–3] Various types of conventional contact temperature sensors, including liquid thermometers, pressure thermometers, thermistors and thermocouples, have made a mighty advance during the past few decades.[4–6] However, when they are used to capture moving objects or targets on a continuous micro scale, the reliability and accuracy of their measurement results is still worth improving. The remote detection technology developed from temperature-sensitive luminescent materials can effectively make up for the shortcomings of contact temperature sensors and plays a more and more critical role in many scenes.[7,8] It indicates the temperature change by monitoring optical signals such as wavelength, bandwidth, fluorescence lifetime and luminescence intensity ratio (LIR). Among them, LIR is less affected by the external environment, which is an ideal technical index for designing a high-precision and reliable optical temperature sensor.[9,10]

The LIR-based thermometry relies on at least two discrete emission peaks with a large difference in temperature response. Early studies focus on the thermally coupled energy levels (TCLs) of lanthanide ions.[11,12] The temperature-dependent luminescence of thermally coupled emitting states provides a strategy for measuring the change in temperature. However, the energy gap between the thermally coupled energy levels of some lanthanide ions is not wide enough (200–2000 cm^{-1}) (e.g., $^2H_{11/2}$-$^4I_{15/2}$ and $^4S_{3/2}$-$^4I_{15/2}$ of Er^{3+}) or even overlaps with each other to a certain extent, resulting in low signal discriminability.[13–16] Moreover, it should be noted that the narrow energy gap of TCLs corresponds to low relative temperature sensitivity (S_r), that is, the temperature-sensitive luminescent materials developed based on this concept usually suffer from the problems of low sensitivity, poor signal discrimination and large detection error. As an alternative, multiple luminescent thermometers benefit from two or more luminescence bands with diverse thermal responses, which has been proved to be

☆ **Foundation item:** Project supported by the Central Funding Project for Local Science and Technology Development (2022JH6/100100048), the National Natural Science Foundation of China (52103038), and Shenyang Science and Technology Plan Project (20-202-1-12).

* Corresponding author.
** Corresponding author.
E-mail addresses: wzy@syu.edu.cn (Z. Wang), H.T.Hintzen@tudelft.nl (H.T. Hintzen).

https://doi.org/10.1016/j.jre.2023.06.017
1002-0721/

an effective means of temperature measurement.[17] Divalent and trivalent europium, which have almost the opposite responses to temperature, are a pair of activators commonly used in fluorescent thermometers. In recent years, the research on Eu^{2+}-Eu^{3+} co-activated thermo-sensitive phosphors has made great progress.[18–21] For example, Li et al.[22] reported the excellent tunable sensitivity of $La_{1-y}Gd_yAlO_3$:Eu^{2+},Eu^{3+}, a ratiometric optical thermometer, whose S_r could be as high as 3.233%/K at 303 K. And at the same time, they noticed the abnormal thermal quenching of Eu^{2+} and Eu^{3+} in $La_{1-y}Gd_yAlO_3$, and attributed it to the thermal-activated energy transfer from Eu^{2+} to Eu^{3+}. Similar phenomena can also be found in $LaAlO_3$,[23] $BaMgP_2O_7$[18] and $Sr_3P_4O_{13}$[24] co-activated by Eu^{2+} and Eu^{3+}. We believe that the combination of thermo-responses and energy transfer from Eu^{2+} to Eu^{3+} is a way to improve the sensitivity over a wider temperature range. Furthermore, the emission peak positions generated by the electronic transitions in the Eu^{3+} 4f orbit are relatively fixed in different lattice environments (i.e., orange emission due to $^5D_0 \rightarrow {}^7F_1$ transition from the lattice site with inversion symmetry or red emission due to $^5D_0 \rightarrow {}^7F_2$ transition from the lattice site deviated from the inversion symmetry[25]), while the emission derived from the electronic transitions $4f^65d^1 \leftarrow 4f^7$ ($^8S_{7/2}$) of Eu^{2+} is significantly affected by the surrounding crystal field, which gives us a unique strategy to design the energy gap between multiple emissions or even regulate the sensitivity by screening host compounds.

According to previous research, the emission band of Eu^{2+} in barium boroaluminate $BaAl_2B_2O_7$ extends from near ultraviolet to blue.[26] If we can promote the coexistence of Eu^{2+} and Eu^{3+} in a single $BaAl_2B_2O_7$ host lattice, it is expected to obtain a thermo-sensitive phosphor with ultra-wide energy gap (>10000 cm^{-1}) and superior signal discriminability. Therefore, in this contribution, starting from the solid-state preparation of the phosphors $BaAl_2B_2O_7$:Eu^{3+} and $BaAl_2B_2O_7$:Eu^{2+},Eu^{3+}, we focused on the luminescence and the thermosensitive properties of the phosphor $BaAl_2B_2O_7$:Eu^{2+},Eu^{3+}, and finally summarized and put forward a design strategy to improve the thermosensitive performance of Eu^{2+}-Eu^{3+} co-activated luminescent materials.

2. Experimental

2.1. Materials and preparation

$BaAl_2B_2O_7$:Eu phosphors were prepared by the high-temperature solid-state reaction in two ways, either in ambient air or carbothermally. In order to ensure that Eu^{2+} and Eu^{3+} coexist in the matrix lattice and have a suitable relative emission intensity, the total doping concentration of europium was fixed at 2 mol%.[27] The raw materials were $BaCO_3$ (Aladdin, A.R.), Al_2O_3 (Aladdin, A.R.), H_3BO_3 (Aladdin, A.R.), and Eu_2O_3 (Aladdin, 99.99%) taken according to the stoichiometric ratio. The mixed raw materials were continuously ground in an agate mortar for 40 min to homogenization and transferred to the 5 mL corundum crucibles. The crucible for the carbothermal reaction was placed in another 20 mL crucible. The space in between was filled with activated charcoal powder (Macklin, A.R.) so that the internal crucible was completely buried. Then, the crucibles containing the mixtures were heated to 775 °C at 2 °C/min and kept in a muffle furnace for 5 h. After the mixtures were naturally cooled to room temperature, they were removed from the furnace and ground into powder in the agate mortar for subsequent characterization.

2.2. Characterization

The powder X-ray diffraction (XRD) data were obtained on an X-ray diffractometer (Rigaku SmartLab SE, Japan) with Cu Kα radiation ($\lambda = 0.15418$ nm) at a scanning rate of 1 (°)/min at 40 kV and 30 mA. The micrographs, energy dispersive X-ray (EDX) spectroscopy and elemental mappings were taken by a scanning electron microscope (SEM, TESCAN MIRA LMS, Czech) with the accelerated voltage of 30 kV and a transmission electron microscope (TEM, JEOL JEM-2100F, Japan) with the accelerated voltage of 200 kV. The X-ray photoelectron spectroscopy (XPS) was measured on an X-ray photoelectron spectrometer (Thermo Scientific K-Alpha, USA). The diffuse reflectance spectra (DRS) were collected by an ultraviolet–visible spectrophotometer (Shimadzu UV-3600i Plus, Japan) using $BaSO_4$ as the reference standard. The photoluminescence (PL) excitation and emission spectra were measured by a steady-state fluorescence spectrometer (Hitachi F7100, Japan). The fluorescence lifetime and the temperature-dependent emission spectra were measured by another fluorescence spectrometer (Edinburgh FLS1000, Britain) equipped with an electronic temperature regulating device.

3. Results and discussion

3.1. Phase composition and crystal structure

To obtain the phase composition and crystal structure information, X-ray powder diffraction data of the phosphors prepared in air and carbothermal reduction atmosphere were analyzed utilizing the Rietveld refinement based on the GSAS program starting with $BaAl_2B_2O_7$ crystal structure.[28] The refinement results are presented in Fig. 1(a, b) and Table 1, and the refined structural parameters are also given in Table S1. According to rules of substitution, there was only one potential crystallographic site (i.e., Ba with D_3 point symmetry and coordination number of six) for Eu in the structure, so we fixed Eu atoms at Ba site in the refinement process. The refined results show that the two phosphors have a single phase without impurities, implying that Eu^{2+} and/or Eu^{3+} ions are doped at an atomic level. The profile values of R_{wp} (8.78%–9.21%) and R_p (5.93%–7.60%) are within the reasonable and credible range, indicating that the refined crystal structures of the phosphors match well with the initial structural model of $BaAl_2B_2O_7$. Additionally, the schematic fragments of the refined structures viewed along 100 directions are exhibited in Fig. 1(c). The [BaO_6] pentahedrons build layers along the 100 direction and are connected with [AlO_4] tetrahedrons by sharing the oxygen atoms at the corners. B^{3+} is bonded in a trigonal planar geometry to three equivalent O^{2-} atoms.

3.2. Micromorphology

The micromorphologies of $BaAl_2B_2O_7$:Eu phosphors prepared carbothermally (Fig. 2(a, b, d, e) and in ambient air (Fig. S1) were investigated by SEM technique. The micromorphologies of the particles of the two phosphors prepared in different atmospheres are quite similar, showing irregular shapes and agglomeration to a certain extent. Considering that there was no further industrialized crushing and screening, the particle size of the phosphor obtained was not uniform. The average particle size was estimated to be about 20 μm, according to the images. EDX characterization of the particle within the image range of Fig. 2(e) proved that the phosphor contained Ba, Al, Eu and O elements (Fig. 2(c)), and the doped Eu is evenly distributed on the surface and in the bulk of phosphor particles as other intrinsic elements (Fig. 2(f–i)). Since the peak position of B element was difficult to distinguish from other elements in the low-energy region, it was not qualitatively detected here.

Fig. 3(a, b) are the TEM and high-resolution TEM (HRTEM) images of a $BaAl_2B_2O_7$:Eu particle prepared carbothermally, which

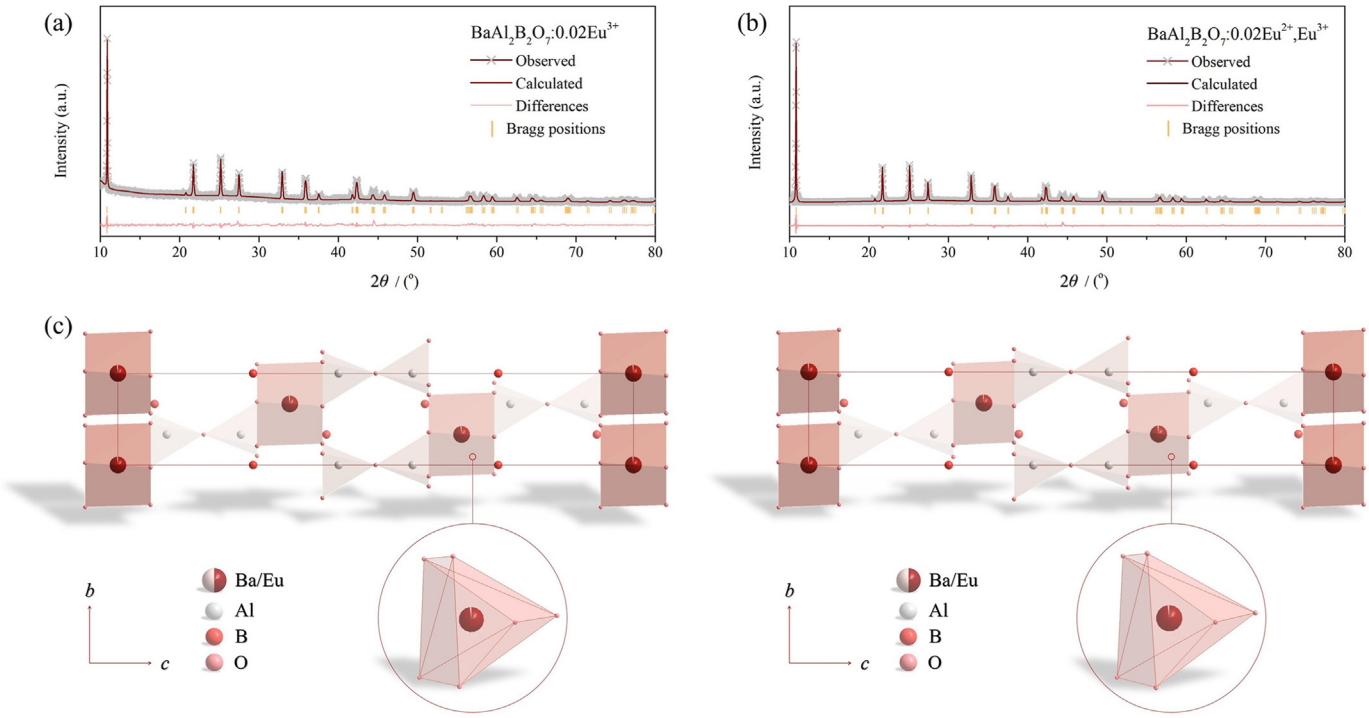

Fig. 1. Rietveld refinement of $BaAl_2B_2O_7$:Eu prepared in ambient air (a) and carbothermally (b); (c) Crystal structures of $BaAl_2B_2O_7$:Eu based on the refined results.

Table 1
Rietveld refinement parameters of $BaAl_2B_2O_7$:Eu^{3+} and $BaAl_2B_2O_7$:Eu^{2+},Eu^{3+} phosphors.

Compound	$BaAl_2B_2O_7$:Eu^{3+}	$BaAl_2B_2O_7$:Eu^{2+},Eu^{3+}
a (nm)	0.50105	0.50098
c (nm)	2.4452	2.4471
α (°)	90.000	90.000
β (°)	90.000	90.000
γ (°)	120.00	120.00
V (nm^3)	0.53164	0.53180
χ^2	1.92	3.38
R_{wp}	8.78%	9.21%
R_p	5.93%	7.60%

illustrates no apparent structural defects in the selected region, and the sample was highly crystallized. The lattice fringe with the d spacing of 0.4236 nm could be assigned to the (101) crystal plane. The value of $d_{(101)}$ was slightly reduced compared with undoped $BaAl_2B_2O_7$ (i.e., $d_{(101)} = 0.4264$ nm) after the substitution of Eu for Ba ions because the ionic radii of Eu^{2+} ($r = 0.117$ nm) and Eu^{3+} ($r = 0.095$ nm) are smaller than that of Ba^{2+} ($r = 0.135$ nm) (All coordination numbers are 6).[29]

3.3. Coexistence of Eu^{2+} and Eu^{3+}

The presence of Ba, Al, O and Eu elements in the phosphors can be reconfirmed in the XPS spectrum (Fig. 4(a, b)). In contrast to EDX, with XPS it is possible to demonstrate the presence of B. According to XPS, Eu in both phosphors is present in the trivalent Eu^{3+} state (1163.6 eV). Compared with the $BaAl_2B_2O_7$:Eu phosphor prepared in the air atmosphere, the characteristic signal of Eu^{2+} in $BaAl_2B_2O_7$:Eu phosphor prepared in the carbothermal environment can be additionally detected in the high-resolution XPS spectrum (1156.4 eV) (Fig. 4(c, d)), which means that the carbothermal environment promotes the partial reduction of Eu^{3+} in the host lattice. In previous studies, partial reduction of Eu^{3+} in $BaAl_2B_2O_7$ can also be realized in ambient air by solid-state reaction,[27] which seems to be contrary to our results but also well understood, because the self-reduction of Eu^{3+} is determined by a variety of factors (including Eu ion doping concentration, synthesis temperature, holding time, etc.).[30] Therefore, carbothermal reaction was adopted in our case to ensure the stable coexistence of Eu^{2+} and Eu^{3+} in the host lattice.

3.4. Diffuse reflectance spectra

The UV-Vis diffuse reflectance spectra of $BaAl_2B_2O_7$:Eu^{3+} and $BaAl_2B_2O_7$:Eu^{2+},Eu^{3+} phosphors are presented in Fig. 5. For the $BaAl_2B_2O_7$:Eu^{3+} phosphor prepared in the air atmosphere (black curve), we can observe that the absorption band with the prominent peak at about 260 nm is attributed to the $O^{2-} \rightarrow Eu^{3+}$ charge transfer band (CTB). The absorption peak at 394 nm originates from the $^7F_0$-$^5L_6$ electronic transitions of Eu^{3+}. Correspondingly, for the $BaAl_2B_2O_7$:Eu^{2+},Eu^{3+} phosphor (red curve) prepared in the carbothermal reduction atmosphere, in addition to the $O^{2-} \rightarrow Eu^{3+}$ charge transfer absorption peak, there is a conspicuous absorption band from $4f^65d^1 \leftarrow 4f^7$ electronic transitions of Eu^{2+} between 330 and 450 nm, which is not reflected in the black curve. It is also worth noting that in this case, the intensity of the $O^{2-} \rightarrow Eu^{3+}$ charge transfer absorption peak is weaker than that of the phosphor obtained in the air atmosphere, indicating that Eu^{3+} in the host compound is partially reduced to Eu^{2+}.

3.5. Photoluminescence properties

To better understand the luminescence characteristics of Eu^{3+} in $BaAl_2B_2O_7$, we first studied the $BaAl_2B_2O_7$:Eu^{3+} phosphor, and its PL spectrum is shown in Fig. S2(a). Under the excitation wavelength at

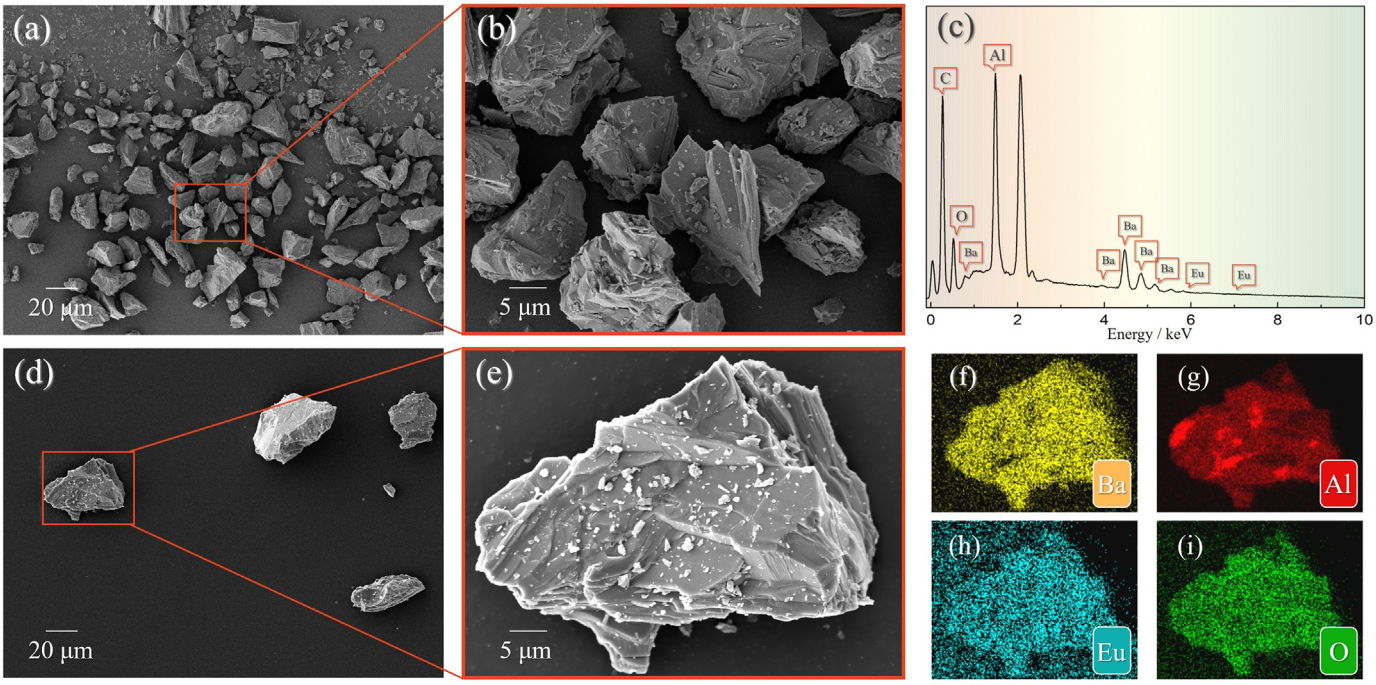

Fig. 2. SEM images with 1000 × (a, c) and 5000 × (b, d) magnifications; EDX spectroscopy (e) and elemental mapping (f–i) images of $BaAl_2B_2O_7$:Eu^{2+},Eu^{3+} phosphor.

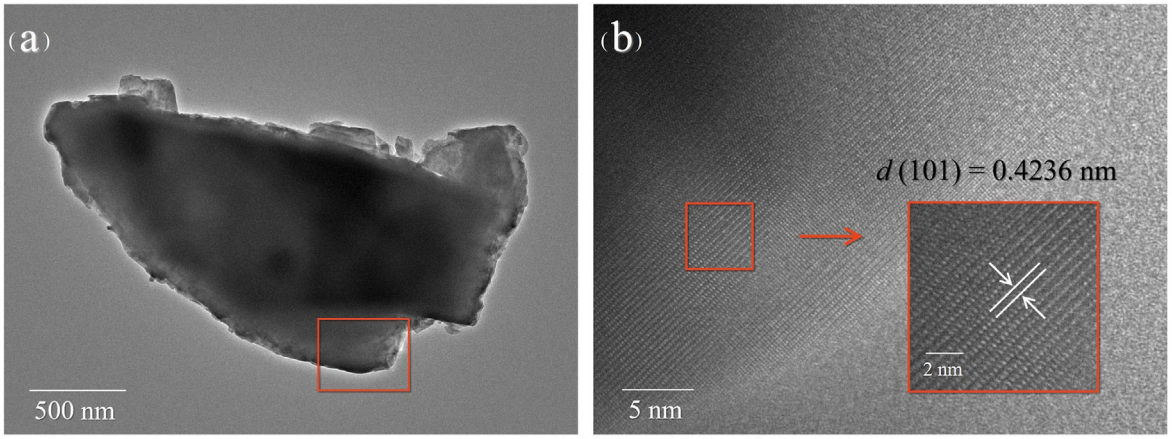

Fig. 3. TEM (a) and HRTEM (b) images of the selected region of a $BaAl_2B_2O_7$:Eu phosphor particle prepared in carbothermic reducing atmosphere.

394 nm, the emission spectrum contains a series of narrow peaks, respectively attributed to the $^5D_0 \rightarrow {}^7F_J$ (J = 0, 1, 2, 3, 4) electronic transitions of Eu^{3+}. It is known that the magnetic dipole transition ($^5D_0 \rightarrow {}^7F_1$) of Eu^{3+} will be dominant if Eu^{3+} ions are located at the sites with inversion symmetry. In contrast, the electric dipole transition ($^5D_0 \rightarrow {}^7F_2$) will be prevalent due to the absence of inversion symmetry.[25] The dominant peak ($^5D_0 \rightarrow {}^7F_2$) in the emission spectrum is located at 614 nm, implying that the Eu^{3+} luminescence center is located on a lattice site deviating from the inversion symmetry (i.e., 3*a* sites with D_3 point symmetry of Ba), and the electric dipole transition is the primary factor in this luminescence process.[31] Typically, the emission intensity from the $^5D_0 \rightarrow {}^7F_3$ forbidden transition (at about 655 nm) is weak. Still, for $BaAl_2B_2O_7$:Eu^{3+}, also the $^5D_0 \rightarrow {}^7F_4$ emission (at about 705 nm) has low intensity, indicating a low symmetry of coordination geometry around the Eu^{3+}.[32] The relatively weak $^5D_0 \rightarrow {}^7F_4$ transition is beneficial for lumen efficiency because of the low sensitivity of the human eye in this spectral region.[33] Monitored by 614 nm wavelength ($^5D_0 \rightarrow {}^7F_2$ emission), the excitation spectrum of the phosphor involves two parts (Fig. S2(a)). One is the excitation band between 200 and 300 nm, which comes from the electronic transition from $2p^6$ states of O^{2-} to $4f^6$ states of Eu^{3+}, and agrees with the absorption peak at about 260 nm in the reflection spectrum (Fig. 5), while the other is a range of narrow excitation peaks between 300 and 550 nm corresponding to the 4f-4f ($^5H_6 \leftarrow {}^7F_0$, $^5D_4 \leftarrow {}^7F_0$, $^5G_4 \leftarrow {}^7F_0$, $^5L_7 \leftarrow {}^7F_0$, $^5L_6 \leftarrow {}^7F_0$, $^5D_2 \leftarrow {}^7F_0$, $^5D_1 \leftarrow {}^7F_0$ and $^5D_1 \leftarrow {}^7F_1$) electronic transitions of Eu^{3+}. The above shows that the phosphor can be effectually pumped by deep/near UV and visible blue light.

The fluorescent decay curve of Eu^{3+} emission at 614 nm excited at 394 nm in $BaAl_2B_2O_7$:Eu^{3+} is shown in Fig. S2(c). The lifetime τ can be calculated according to the following double exponential equation[34]:

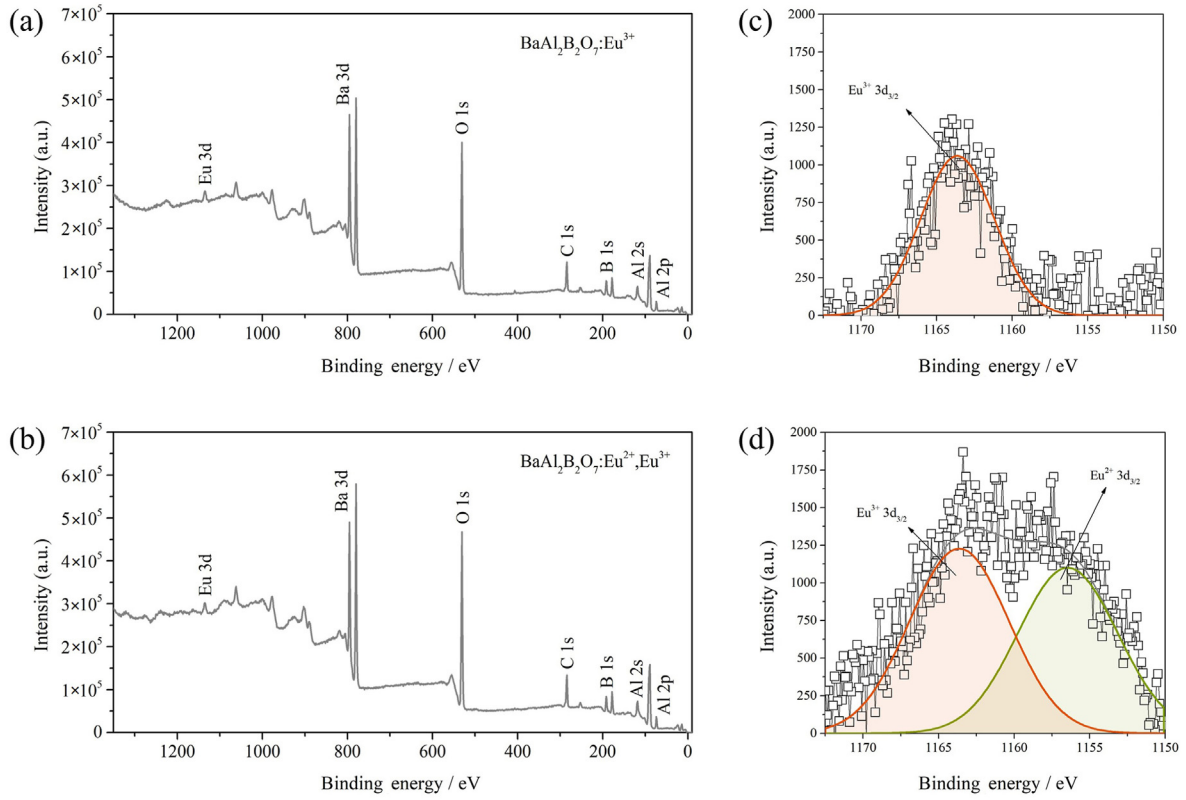

Fig. 4. XPS survey spectra of $BaAl_2B_2O_7:Eu^{3+}$ (a) and $BaAl_2B_2O_7:Eu^{2+},Eu^{3+}$ (b) phosphors; (c, d) Core level spectra of Eu $3d_{3/2}$ of the corresponding phosphors.

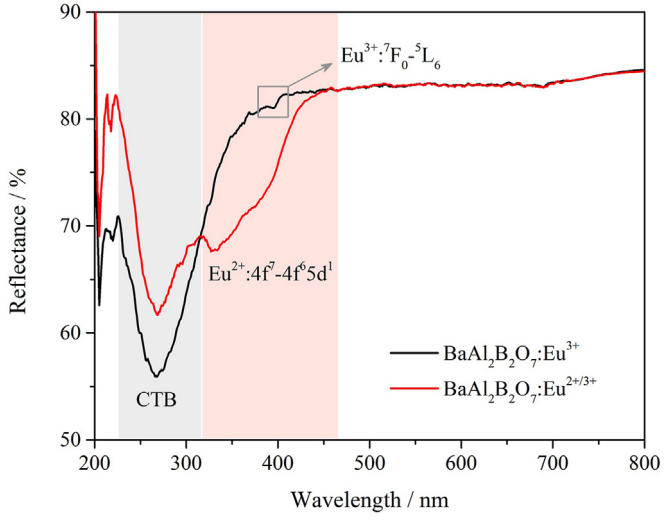

Fig. 5. UV-Vis diffuse reflectance spectra of $BaAl_2B_2O_7:Eu^{3+}$ and $BaAl_2B_2O_7:Eu^{2+},Eu^{3+}$ phosphors.

$$I(t) = I_0 + A_1 \exp\left(-\frac{t}{\tau_1}\right) + A_2 \exp\left(-\frac{t}{\tau_2}\right) \quad (1)$$

In the equation above, $I(t)$ means the emission intensity at time t. A_1 and A_2 are constants. τ_1 and τ_2 are lifetimes for the exponential components. The average lifetime can be calculated as:

$$\tau = \left(A_1\tau_1^2 + A_2\tau_2^2\right) \Big/ \left(A_1\tau_1 + A_2\tau_2\right) \quad (2)$$

The fluorescent lifetime of Eu^{3+} at 614 nm is determined to be 1.95 ms, which is a typical value for an electric dipole allowed $^5D_0 \rightarrow {}^7F_2$ emission.[25] To describe the emission color of $BaAl_2B_2O_7:Eu^{3+}$ more clearly from the application point of view, the CIE chromaticity coordinates of $BaAl_2B_2O_7:Eu^{3+}$ phosphor (λ_{ex} = 394 nm) are presented in the chromaticity diagram (Fig. S2(d)). The color coordinates of $BaAl_2B_2O_7:Eu^{3+}$ phosphor are (0.6081, 0.3867) in the reddish-orange region of the CIE chromaticity diagram. Based on the standard of NTSC and European Broadcasting Union (EBU), the color purity, as another critical factor for monochromatic light, has been calculated according to the following equation[35]:

$$\text{Color purity} = \frac{\sqrt{(x - x_i)^2 + (y - y_i)^2}}{\sqrt{(x_d - x_i)^2 + (y_d - y_i)^2}} \times 100\% \quad (3)$$

where (x, y), (x_i, y_i) and (x_d, y_d) stand for the CIE chromaticity coordinates of studied $BaAl_2B_2O_7:Eu^{3+}$ phosphor (0.6081, 0.3867), white illumination (0.3333, 0.3333) and dominant emission wavelength (0.6136, 0.3872), respectively. Calculation demonstrates that the color purity can be as high as 98.2%, which is higher than those of commercial Eu^{3+}-activated reddish-orange-emitting phosphors, such as $Y_2O_2S:Eu^{3+}$ (94.3%),[36] indicating that the emission color of $BaAl_2B_2O_7:Eu^{3+}$ is extremely close to the spectral edge of the 1931 CIE chromatic diagram due to the dominant $^5D_0 \rightarrow {}^7F_2$ line transition of Eu^{3+}. In addition, it is known that the color temperature determines the lighting and visual effects, so the correlated color temperature (CCT) of the phosphor was further studied by McCamy's approximate function[37]:

$$CCT = -449\left(\frac{x-x_e}{y-y_e}\right)^3 + 3525\left(\frac{x-x_e}{y-y_e}\right)^2 - 6823.3\left(\frac{x-x_e}{y-y_e}\right) + 5520.33 \quad (4)$$

where (x_e, y_e) are chromaticity epicenter (0.3322, 0.1863). Therefore, we calculated that the CCT of $BaAl_2B_2O_7:Eu^{3+}$ phosphor is 2815 K.

To realize the coexistence of Eu^{2+} and Eu^{3+} in the $BaAl_2B_2O_7$ system, $BaAl_2B_2O_7:Eu^{2+},Eu^{3+}$ phosphor was prepared by the carbothermal reaction, and its luminescence properties were investigated. The emission peak from $4f^65\,d^1 \rightarrow 4f^7$ electronic transitions of Eu^{2+} was observed under 288 nm UV excitation to be located around 375 nm (Fig. 6(a)). In Fig. 6(b), we found the narrow-line emission corresponding to the 4f-4f electronic transitions of Eu^{3+} under 394 nm UV excitation, similar to $BaAl_2B_2O_7:Eu^{3+}$ (Fig. S2(a)). The PL excitation spectra monitored at 375 and 614 nm are plotted in Fig. 6(c, d), respectively. The wide excitation band in Fig. 6(a) is derived from the $4f^65d^1 \leftarrow 4f^7$ transitions of Eu^{2+}. The excitation spectrum monitored at 614 nm consists of CTB and intra-configurational 4f-4f transitions of Eu^{3+}.

Furthermore, we investigated the fluorescence lifetime of Eu^{2+} and Eu^{3+} in $BaAl_2B_2O_7:Eu^{2+},Eu^{3+}$ phosphor (Fig. S3 and Fig. 6(e)). The lifetime of Eu^{3+} is calculated to be 1.38 ms, smaller than that of Eu^{3+} in $BaAl_2B_2O_7:Eu^{3+}$ (i.e., 1.95 ms). The lifetime of Eu^{2+} is calculated to be 0.96 μs. To visualize the influence of Eu^{2+} on the luminous color of the phosphor, the CIE chromaticity coordinates of $BaAl_2B_2O_7:Eu^{2+},Eu^{3+}$ are given in Fig. 6(f). The color coordinates of $BaAl_2B_2O_7:Eu^{2+},Eu^{3+}$ are calculated to be (0.2362, 0.1161) upon the excitation at 288 nm.

3.6. Ratiometric thermo-response of Eu^{2+} and Eu^{3+}

As mentioned above, the luminescence behavior of Eu^{2+} and Eu^{3+} in $BaAl_2B_2O_7:Eu^{2+},Eu^{3+}$ depends largely on the applied excitation wavelengths. On this premise, we further explored the ratiometric thermo-response of Eu^{2+} and Eu^{3+} and the temperature-sensitive luminescence properties of the phosphor. Eu^{2+} and Eu^{3+} in the host lattice were simultaneously pumped by a deep UV with a wavelength of 249 nm. The temperature-dependent emission spectrum and the histogram of luminescence intensity variations of Eu^{2+} ($4f^65d^1 \rightarrow 4f^7$) and Eu^{3+} ($^5D_0 \rightarrow {}^7F_2$) on the dependence of operating temperatures are plotted in Fig. 7(a) and (b), respectively. It can be seen that both Eu^{2+} and Eu^{3+} show pronounced thermal quenching in $BaAl_2B_2O_7:Eu^{2+},Eu^{3+}$ phosphor, that is, their luminescence intensity decreases gradually with the increase of operating temperature. However, it is worth noting that the decreasing trend of the luminous intensity of Eu^{3+} seems to be linear, whereas the luminous intensity of Eu^{2+} shows a lower change rate at the initial stage of heating up, and subsequently intensifies with the increase of temperature. Therefore, the different thermal responses of Eu^{2+} and Eu^{3+} make it possible to develop the temperature-sensing function of $BaAl_2B_2O_7:Eu^{2+},Eu^{3+}$ phosphor.

The relation between LIR (I^{3+}_{Eu}/I^{2+}_{Eu}) and operating temperature from 298 to 473 K can be fitted piecewise by the following equation[38]:

$$LIR = \frac{I_{Eu^{3+}}}{I_{Eu^{2+}}} = A\exp\left(-\frac{\Delta E}{kT}\right) + C \quad (5)$$

where I^{3+}_{Eu} and I^{2+}_{Eu} represent the emission intensities of Eu^{3+} ($^5D_0 \rightarrow {}^7F_2$ emission) and Eu^{2+} ($4f^65d^1 \rightarrow 4f^7$ emission); A, C and ΔE

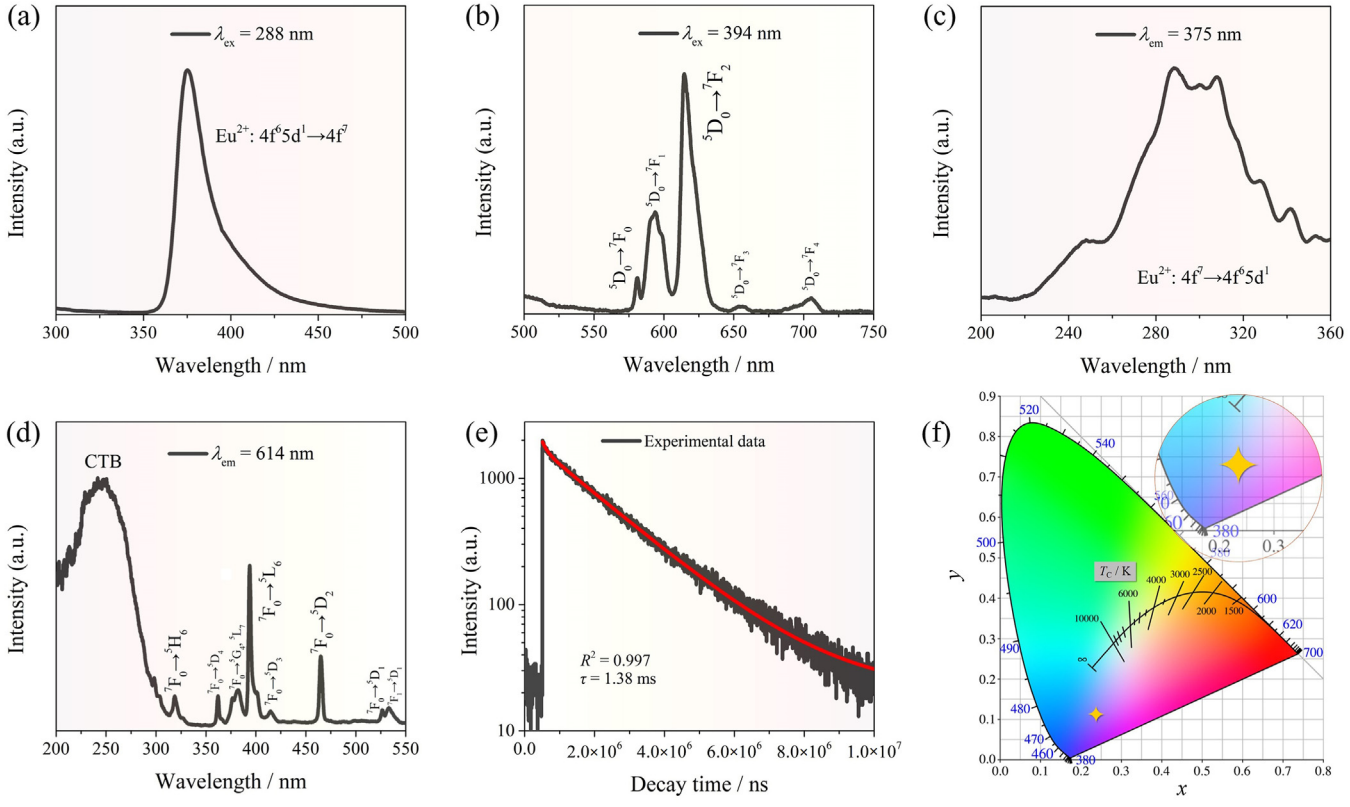

Fig. 6. PL emission (a, b) and excitation (c, d) spectra; (e) Fluorescent decay curve of Eu^{3+} emission at 614 nm; (f) CIE chromaticity coordinates for excitation with 288 nm of $BaAl_2B_2O_7:Eu^{2+},Eu^{3+}$ phosphor. Inset of (f) shows the partial enlarged detail.

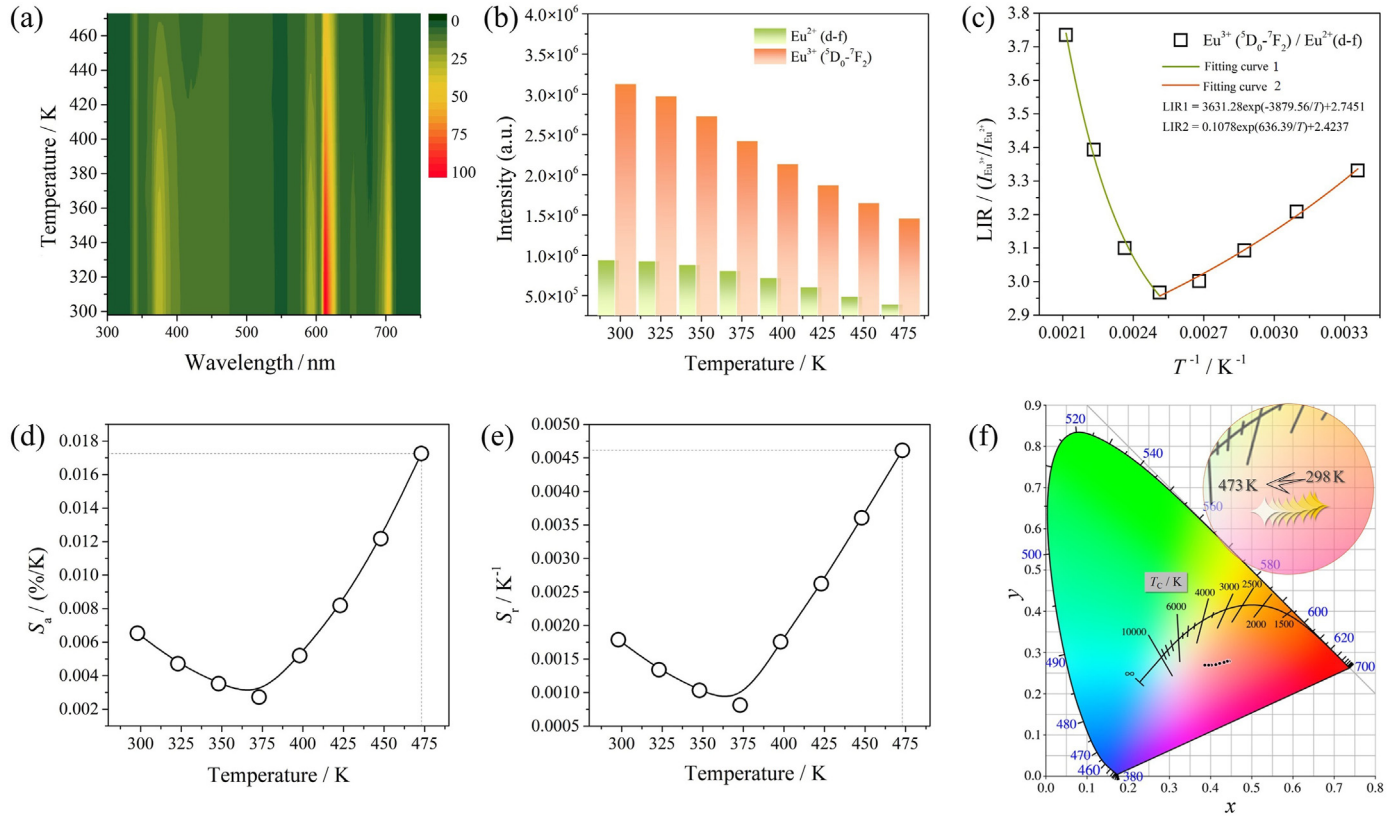

Fig. 7. Temperature-dependent PL spectrum (a) and luminescence intensity variations of Eu^{2+} ($4f^65\ d^1 \rightarrow 4f^7$) and Eu^{3+} ($^5D_0 \rightarrow {}^7F_2$) (b) for excitation with 249 nm; (c) LIR fitting curves; (d, e) Dependence of S_a and S_r on operating temperature; (f) CIE chromaticity coordinates of $BaAl_2B_2O_7:Eu^{2+},Eu^{3+}$ phosphor at different temperatures for excitation with 249 nm.

are parameters related to the constants of Eu^{2+} and Eu^{3+}; k is the Boltzmann constant ($1.3806488 \times 10^{-23}$ J/K), and T is the sample temperature when detecting the emission intensity. The piecewise fitting curves of LIR on the dependence of the operating temperature are plotted in Fig. 7(c). All LIR data points can be adequately fitted by Eq. (5) with a positive ΔE in the temperature range below 398 K and a negative ΔE in the temperature range above 398 K. On this basis, we can further obtain the information on S_a, S_r and temperature uncertainty (δT) through the following equations[38]:

$$S_a = \frac{d(LIR)}{dT} = A \exp\left(-\frac{\Delta E}{kT}\right) \times \frac{\Delta E}{kT^2} \quad (6)$$

$$S_r = \frac{1}{LIR} \times \frac{d(LIR)}{dT} = \frac{A \exp\left(-\frac{\Delta E}{kT}\right)}{A \exp\left(-\frac{\Delta E}{kT}\right) + C} \times \frac{\Delta E}{kT^2} \quad (7)$$

$$\delta T = \frac{1}{S_r} \times \frac{\delta LIR}{LIR} \quad (8)$$

The undetermined variables in Eqs. (6) and (7) can be found from the fitting results in Fig. 7(c). Therefore, the calculated correlation curves of S_a and S_r concerning the operating temperature are shown in Fig. 7(d) and (e), respectively. The maximum value of S_a can be as high as 0.0173 K^{-1} with the operating temperature at 473 K, while the value of S_r can be up to 0.461%/K. These two values have been higher than those of some previously reported representative rare-earth co-doped phosphors (e.g., $YF_3:Eu^{3+}/Tb^{3+}$, $S_r = 0.13\%/K$)[39] and some Eu^{2+}-Eu^{3+} activated phosphors (e.g., $Li_2CaSiO_4:Eu^{2+}/Eu^{3+}$, $S_a = 0.0025\ K^{-1}$, $S_r = 0.298\%/K$).[39] The temperature uncertainty can be evaluated according to Eq. (8), where $\delta LIR/LIR$ is a parameter related to the detecting setup. For the Edinburgh FLS1000 spectrometer used in the measurement, the $\delta LIR/LIR$ value can be up to 0.03%.[40] Thus, the value of δT is approximately between 0.065 and 0.369 K, corresponding to the S_r of 0.081% (at 373 K) to 0.461%/K. This estimated δT is close to the value (0.146–0.352 K, $Eu^{2+}/{}^7F_2$) of $Li_2CaSiO_4:Eu^{2+}/Eu^{3+}$ in Ref. 38.

The CIE chromaticity diagram and the color coordinates of the phosphor collected at different temperatures are plotted in Fig. 7(f) and summarized in Table S2. The color coordinates of the yellowish-pink-emitting phosphor moved towards the white region when the operating temperature increased from 298 to 473 K. The ultra-high signal discriminability ($\Delta\nu$ ~10380 cm^{-1}) can be realized additionally as a consequence of the well-separated typical emission peaks of Eu^{2+} (375 nm) and Eu^{3+} (614 nm), which makes the spectral signals easier to be identified in practical temperature-sensing applications. Nevertheless, it should be recognized that the aforementioned indicators related to temperature sensing can be further optimized by adjusting the chemical composition and crystal structure of the phosphor.

As far as we know, the reason for the great difference in temperature-sensitive behavior between Eu^{2+} and Eu^{3+} ($I_{298\ K}/I_{473\ K} = 2.43$ and 2.15 for Eu^{2+} and Eu^{3+}, respectively) lies in the fact that, on the one hand, the f–f transition of Eu^{3+} is shielded by the fully filled outer 5s and 5p orbits, and its luminescence behavior is weakly affected by the external factors such as temperature or coordination environment, while the 5d electrons in the outer layer of Eu^{2+} are exposed and vulnerable to the influence

of crystal field; On the other hand, the energy quenching paths of Eu^{2+} and Eu^{3+} are entirely different. For Eu^{2+}, during the excitation process corresponding to the 4f-5d parity-allowed transition, the transition of the outer electron from 4f to the outer 5d orbit is accompanied by the contraction of the central ion.[41] According to the configuration coordinate model (Fig. 8), the equilibrium position of the Eu^{2+} 5d excited state is on the left of the 4f ground state equilibrium position, and so the energy can be transferred non-radiatively from the 5d excited state to the 4f ground state through intersection of 5d state with the 4f state. Consequently, the activation energy (ΔE) as related to the distance between the equilibrium position of the excited state and the ground state (ΔR) determines the thermal quenching behavior of Eu^{2+}. For example, when the size of the replaced ions is larger than that of Eu^{2+}, the adjacent ions in the host lattice will inhibit the contraction of the central Eu^{2+} ions, resulting in a smaller difference between the equilibrium distances of the excited state and the ground state and consequently a higher activation energy, which appears as the weaker thermal quenching of Eu^{2+} emission.[42] For the luminescence process of Eu^{3+} in general, after the excitation of Eu^{3+} in the $O^{2-} \rightarrow Eu^{3+}$ charge transfer band, the energy relaxes from the higher energy level to $^5D_0$ state and is released by the characteristic emission of Eu^{3+}. However, in case the charge transfer band is at a lower energy position, there may be a non-radiative transition path from $^5D_0$ excited state to $^7F_0$ ground state through crossing point with charge transfer state (CTS).[43] This potential relaxation path can be further clarified from the configuration coordinate diagram: after the excitation energy reaches the position of the charge transfer band, it relaxes directly to the intersection of the CTS parabola and the ^7F_J manifold; If the energy at the intersection of CST and ^7F_J manifold is higher than the excitation point of CTS, thermal activation is required to complete the radiationless decay. The latter activation process is temperature-dependent, so the luminescence will weaken with the increase of temperature. The charge transfer energy is related to the substituted ions, that is, when Eu^{3+} is placed at a larger lattice site, the charge transfer state shifts to lower energy under the influence of a low electric potential, resulting in smaller activation energy and more substantial thermal quenching.

In this case of $BaAl_2B_2O_7$, Ba^{2+} substituted by europium ion is obviously a "large" lattice site, whether among the IIA elements (r_{Ca} (0.100 nm) < r_{Sr} (0.118 nm) < r_{Ba} (0.135 nm)) or compared with Eu^{2+} (r = 0.117 nm) and Eu^{3+} (r = 0.095 nm) (all coordination numbers are 6),[29] which results in the different thermal quenching behavior of Eu^{2+} and Eu^{3+} in the initial stage of heating up. The quenching rate here is defined as the change in emission intensity per unit temperature. With the further increase in the operating temperature, the quenching rate of Eu^{3+} begins to slow down (Fig. S4), which is consistent with the trend of LIR curve in Fig. 7(c). Similar quenching phenomena have been reported in previous publications.[22,24] It can be speculated that this is due to the energy transfer from Eu^{2+} to Eu^{3+}. The overlap of emission spectrum of Eu^{2+} (375 nm, corresponding with about 26650 cm^{-1}) with the excitation levels of Eu^{3+} ($^5G_5$, $^5G_6$) indicates the inevitable energy transfer from Eu^{2+} to Eu^{3+} in $BaAl_2B_2O_7$ (Fig. S5), which has been verified in previous studies.[44] The average distance (R_a) between donor (Eu^{2+}) and acceptor (Eu^{3+}) can be estimated according to the following equation by Blasse[43]:

$$R_a \approx 2\left(\frac{3V}{4\pi x_c N}\right)^{\frac{1}{3}} \quad (9)$$

where V is the volume of the unit cell, x_c the critical concentration of activator ions, N the number of activator ions per unit cell. Using as input values $V = 0.53120\ nm^3$, $N = 3$ and $x_c = 0.02$, the calculated value of R_a is about 2.57 nm. It should be noted that the distance between the two activator ions on the layered structure along the (100) direction is significantly smaller than that between the layers along the (001) direction, that is, the actual distance between the donor and the acceptor may be even smaller. The energy transfer from Eu^{2+} to Eu^{3+} is attributed to the electric multipole interaction.

The scheme of the energy transfer process is illustrated in Fig. 9. Eu^{2+} ions are excited from $4f^7$ ground state to the $4f^65d^1$ excited state after absorbing ultraviolet radiation energy. Part of the energy is directly radiatively relaxing from $4f^65d^1$ to $4f^7$ level, accompanied by near UV/visible emission; another portion of the energy is transferred non-radiatively from the Eu^{2+} 5d level to the excited state of Eu^{3+} with similar energy values (e.g., $^5L_6$) and then relaxes to the emitting $^5D_0$ level. The effect of energy transfer can be embodied concretely when the temperature reaches about 373 K, even though the energy transfer is not enough to compensate for the energy loss caused by thermal quenching, so the emission intensity of Eu^{3+} is still decreasing, but at a lower rate. In this way, the

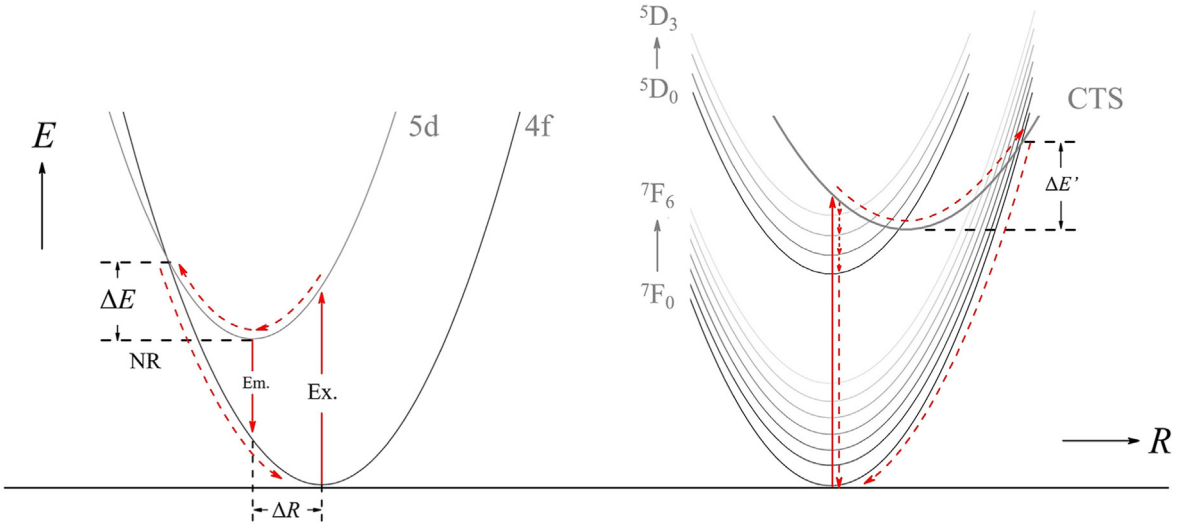

Fig. 8. Schematic configurational coordinate diagram of Eu^{2+} and Eu^{3+} in $BaAl_2B_2O_7$:Eu^{2+},Eu^{3+} phosphor.

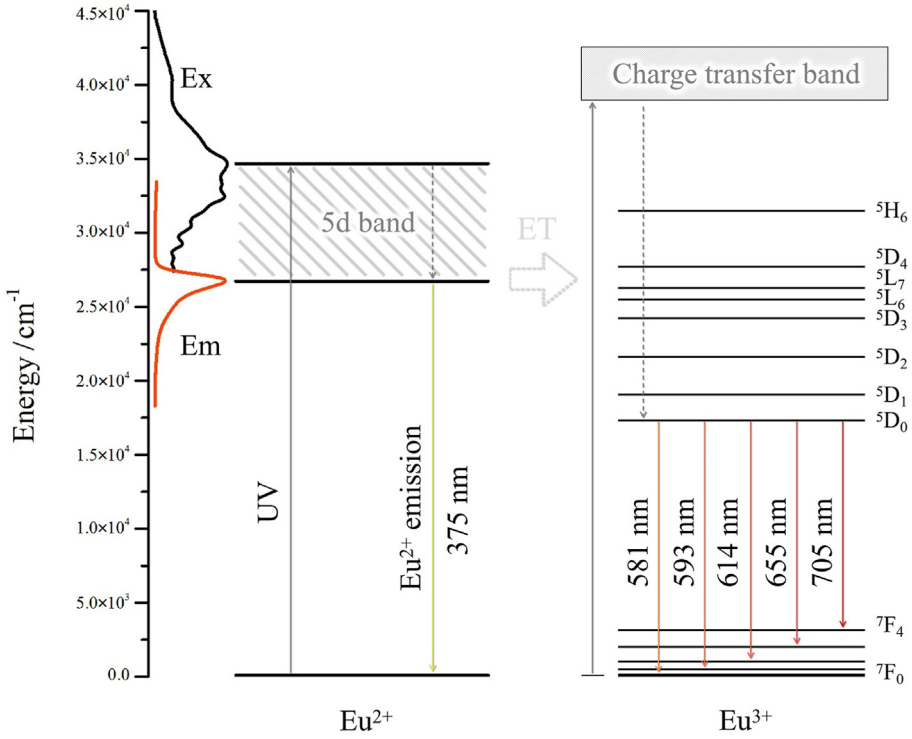

Fig. 9. Schematic diagram of energy level structure of Eu^{2+} and Eu^{3+} in $BaAl_2B_2O_7$ and energy transfer process from Eu^{2+} to Eu^{3+}.

value of LIR depending on $1/T$ is not monotonically decreasing, but presents a segmented distribution.

4. Conclusions

In this contribution, $BaAl_2B_2O_7:Eu^{2+},Eu^{3+}$ phosphor was successfully synthesized by solid-state reaction, and its luminescence and thermo-sensitive properties were systematically studied. The coexistence of Eu^{2+} and Eu^{3+} in the host lattice was triply confirmed by XPS, DRS and PL analysis. Eu^{2+} and Eu^{3+} ions are doped at an atomic level without transforming the crystal structure or introducing hetero-phase. They showed different luminescent thermo-responses under UV excitation, especially at lower sample temperatures. Energy transfer from Eu^{2+} to Eu^{3+} reduces the quenching rate of Eu^{3+} emission with increasing sample temperature, which makes it possible to regulate the thermal sensitivity further. The combination of the above two factors synergistically determines the thermo-sensitive performance of $BaAl_2B_2O_7:Eu^{2+},Eu^{3+}$ phosphor and allows good sensitivity over a wider temperature range. The temperature-dependent emission spectrum shows the excellent performance of the $BaAl_2B_2O_7:Eu^{2+},Eu^{3+}$ phosphor between 298 and 473 K with superior signal discriminability ($\Delta\nu$ ~10380 cm^{-1}) and high sensitivity (S_a = 0.0173 K^{-1}, S_r = 0.461%/K). The study on the photoluminescence and ratiometric thermo-responses of Eu^{2+} and Eu^{3+} in $BaAl_2B_2O_7$ not only provides a phosphor with good properties, but also opens up more possibilities for improving the thermo-sensitive performance of the existing Eu^{2+}-Eu^{3+} co-activated phosphor materials by taking the energy transfer into account.

Declaration of competing interest

The authors declare that they have no conflict of interest.

Acknowledgments

The authors thank Shiyanjia Lab (www.shiyanjia.com) for the TEM analysis.

Appendix A. Supplementary data

Supplementary data to this article can be found online at https://doi.org/10.1016/j.jre.2023.06.017.

References

1. Borisov SM, Vasylevska AS, Krause C, Wolfbeis OS. Composite luminescent material for dual sensing of oxygen and temperature. *Adv Funct Mater*. 2010;16:1536.
2. Stich MIJ, Nagl S, Wolfbeis OS, Henne U, Schaeferling M. A dual luminescent sensor material for simultaneous imaging of pressure and temperature on surfaces. *Adv Funct Mater*. 2008;18:1399.
3. Dils RR. High-temperature optical fiber thermometer. *J Appl Phys*. 1983;54:1198.
4. Tomkins HS, Powell R, Ellis DJ. The pressure dependence of the zirconium-in-rutile thermometer. *J Metamorph Geol*. 2007;25:703.
5. Wendland WM, Armstrong W. Comparison of maximum minimum resistance and liquid-in-glass thermometer records. *J Atmos Ocean Technol*. 1993;10:233.
6. Verma SB, Motha RP, Rosenberg NJ. A comparison of temperature fluctuations measured by a microbead thermistor and a fine wire thermocouple over a crop surface. *Agric Meteorol*. 1979;20:281.
7. Xu W, Zhu X, Zhao D, Zheng LJ, Shang FK, Zhang ZG. Optical thermometry based on near-infrared luminescence from phosphors mixture. *J Rare Earths*. 2022;40:201.
8. Russell PC, Haber R, Jones GR, Mcgrory W. A chromatically addressed optical fiber sensor for non-contact temperature monitoring. *Sens Actuator A Phys*. 1999;76:231.
9. Wang X, Li XP, Yu HQ, Xu S, Sun JS, Cheng LH, et al. Effects of Bi^{3+} on down-/up-conversion luminescence, temperature sensing and optical transition properties of Bi^{3+}/Er^{3+} co-doped $YNbO_4$ phosphors. *J Rare Earths*. 2022;40:381.
10. Wang ZY, Ma GF, Xie CA, Bu XY, Mi RY, Chen J, et al. Dual-driven ratiometric luminescence behaviour of Eu^{2+} and Eu^{3+} in a single host of $SrAl_2O_4$ prepared in ambient atmosphere. *J Alloys Compd*. 2023;941:168912.
11. Zhao L, Cai JJ, Hu FF, Li XY, Cao ZM, Wei XT, et al. Optical thermometry based on thermal population of low-lying levels of Eu^{3+} in $Ca_{2.94}Eu_{0.04}Sc_2Si_3O_{12}$. *RSC Adv*. 2017;7:7198.

12. Suo H, Guo CF, Li T. Broad-scope thermometry based on dual-color modulation up-conversion phosphor $Ba_5Gd_8Zn_4O_{21}:Er^{3+}/Yb^{3+}$. *J Phys Chem C*. 2016;120:2914.
13. Ran W, Noh HM, Park SH, Lee BR, Kim JH, Jeong JH, et al. Application of thermally coupled energy levels in Er^{3+} doped $CdMoO_4$ phosphors: enhanced solid-state lighting and non-contact thermometry. *Mater Res Bull*. 2019;117:63.
14. Bu YY, Yan XH. Temperature dependent photoluminescence of Eu^{3+}-doped $Ca_7V_4O_{17}$. *J Lumin*. 2017;190:50.
15. Zhou SS, Jiang GC, Li XY, Jiang S, Wei XT, Chen YH, et al. Strategy for thermometry via Tm^{3+}-doped $NaYF_4$ core-shell nanoparticles. *Opt Lett*. 2014;39:6687.
16. Cao ZM, Zhou SS, Jiang GC, Chen YH, Duan CK, Yin M. Temperature dependent luminescence of Dy^{3+} doped $BaYF_5$ nanoparticles for optical thermometry. *Curr Appl Phys*. 2014;14:1067.
17. Cheng Y, Gao Y, Huang F, Wang YS. Strategy design for ratiometric luminescence thermometry: circumventing the limitation of thermally coupled levels. *J Mater Chem C*. 2018;6:7462.
18. Li S, Qiu ZX, Mo YH, Zhang HW, Lian HZ, Zhang JL, et al. Self-reduction-induced $BaMgP_2O_7:Eu^{2+/3+}$: a multi-stimuli-responsive phosphor for X-ray detection, anti-counterfeiting and optical thermometry. *Dalton Trans*. 2022;51:6622.
19. Zhou LH, Du P, Li L. Facile modulation the sensitivity of Eu^{2+}/Eu^{3+}-coactivated Li_2CaSiO_4 phosphors through adjusting spatial mode and doping concentration. *Sci Rep*. 2020;10:20180.
20. Huang S, Shang MM, Yan Y, Dang PP, Lin J. Regulation of local site structures to stabilize mixed-valence $Eu^{2+/3+}$ under a reducing atmosphere for multicolor photoluminescence. *Inorg Chem*. 2022;61:1756.
21. Kolesnikov IE, Afanaseva EV, Kurochkin MA, Kolesnikov EY, Lahderanta E. Mixed-valent $MgAl_2O_4:Eu^{2+}/Eu^{3+}$ phosphor for ratiometric optical thermometry. *Physica B*. 2022;624:413456.
22. Li CX, Chen BW, Deng DG, Yu H, Li Hao, Shen CY, et al. A ratiometric optical thermometer with tunable sensitivity and superior signal discriminability based on Eu^{2+}/Eu^{3+} co-doped $La_{1-y}Gd_yAlO_3$ phosphors. *J Lumin*. 2020;221:117036.
23. Chen BW, Li CX, Deng DG, Ruan FP, Wu M, Wang L, et al. Temperature sensitive properties of Eu^{2+}/Eu^{3+} dual-emitting $LaAlO_3$ phosphors. *J Alloys Compd*. 2019;792:702.
24. Yu H, Su WT, Chen LF, Deng DG, Xu SQ. Excellent temperature sensing characteristics of europium ions self-reduction $Sr_3P_4O_{13}$ phosphors for ratiometric luminescence thermometer. *J Alloys Compd*. 2019;806:833.
25. Binnemans K. Interpretation of europium(III) spectra. *Coord Chem Rev*. 2015;295:1.
26. Camardello SJ, Toscano PJ, Brik MG, Srivastava AM. Optical spectroscopy, thermal quenching and electron–vibrational interaction of the octahedrally coordinated Eu^{2+} ion in $CaAl_2B_2O_7$ and $BaAl_2B_2O_7$. *Opt Mater*. 2014;37:404.
27. Palaspagar RS, Gawande AB, Sonekar RP, Omanwar SK. $Eu^{3+} \rightarrow Eu^{2+}$ reduction in $BaAl_2B_2O_7$ phosphor in oxidizing environment. *Optik*. 2015;126:5030.
28. Ye N, Zeng WR, Wu BC, Chen CT. Crystal structure of barium aluminium borate, $BaAl_2B_2O_7$. *Zeitschrift für Kristallographie*. 1998;213:452.
29. Shannon RD. Revised effective ionic radii and systematic studies of interatomic distances in halides and chalcogenides. *Acta Crystallogr D*. 1976;32:751.
30. Pei Z, Zeng Q, Su Q. A study on the mechanism of the abnormal reduction of $Eu^{3+} \rightarrow Eu^{2+}$ in $Sr_2B_5O_9Cl$ prepared in air at high temperature. *J Solid State Chem*. 1999;145:212.
31. Zhang Y, Jia CH, Su ZH, Zhang WF. The enhanced and color-tunable photoluminescence of Eu^{3+}/V^{5+} co-doped $Gd_2Ti_2O_7$ nanocrystals. *J Alloys Compd*. 2009;479:381.
32. Sa Ferreira RA, Nobre SS, Granadeiro CM, Nogueira HI, Carlos LD, Malta OL. A theoretical interpretation of the abnormal $^5D_0 \rightarrow {}^7F_4$ intensity based on the Eu^{3+} local coordination in the $Na_9[EuW_{10}O_{36}]\cdot 14H_2O$ polyoxometalate. *J Lumin*. 2006;121:561.
33. Barten PGJ. Formula for the contrast sensitivity of the human eye. *Proc SPIE*. 2003;5294:231.
34. Mei LF, Liu HK, Liao LB, Zhang YY, Kumar RV. Structure and photoluminescence properties of red-emitting apatite-type phosphor $NaY_9(SiO_4)_6O_2:Sm^{3+}$ with excellent quantum efficiency and thermal stability for solid-state lighting. *Sci Rep*. 2017;7:15171.
35. Wei ZG, Sun LD, Liao CS, Yan CH, Huang SH. Fluorescence intensity and color purity improvement in nanosized YBO_3:Eu. *Appl Phys Lett*. 2002;80:1447.
36. Jiao HY, Wang YH, Zhang JC. Novel red phosphors for light emitting diodes: $Sr_{2-y}Ce_{1-x}Ti_xO_4:yEu^{3+}$. *J Phys Conf Ser*. 2009;152:12089.
37. McCamy CS. Correlated color temperature as an explicit function of chromaticity coordinates. *Color Res Appl*. 1992;17:142.
38. Zhou LH, Du P, Li L. Facile modulation the sensitivity of Eu^{2+}/Eu^{3+}-coactivated Li_2CaSiO_4 phosphors through adjusting spatial mode and doping concentration. *Sci Rep*. 2020;10:20180.
39. Chen DQ, Wang ZY, Zhou Y, Huang P, Ji ZG. Tb^{3+}/Eu^{3+}: YF_3 nanophase embedded glass ceramics: structural characterization, tunable luminescence and temperature sensing behavior. *J Alloys Compd*. 2015;646:339.
40. Zhao D, Zhang SR, Zhang RJ, Liu BZ, Yao QS. Warm white light emission, thermochromic property and long persistent luminescence derived from multi-sites of Eu^{2+}/Eu^{3+} in host lattice. *Chem Eng J*. 2021;428:131023.
41. Dexter DL. Theory of the optical properties of imperfections in nonmetals. *Solid State Phys*. 1958;6:353.
42. Blasse G. Thermal quenching of characteristic fluorescence. *J Chem Phys*. 1969;51:3529.
43. Blasse G. Radiationless transitions in the Eu^{3+} center in $LaAlO_3$. *J Chem Phys*. 1970;53:4450.
44. Dong HJ, Chang SL. Effects of preparation method and flux on luminescent properties of $BaAl_2B_2O_7:Eu^{3+}$. *Rare Met Mater Eng*. 2007;2:359 (in Chin.).